

ARTICLE

Received 8 May 2013 | Accepted 27 Aug 2013 | Published 23 Sep 2013

DOI: 10.1038/ncomms3511

Room-temperature spin-spiral multiferroicity in high-pressure cupric oxide

Xavier Rocquefelte¹, Karlheinz Schwarz², Peter Blaha², Sanjeev Kumar³ & Jeroen van den Brink^{4,5}

Multiferroic materials, in which ferroelectric and magnetic ordering coexist, are of fundamental interest for the development of multi-state memory devices that allow for electrical writing and non-destructive magnetic readout operation. The great challenge is to create multiferroic materials that operate at room temperature and have a large ferroelectric polarization P . Cupric oxide, CuO, is promising because it exhibits a significant polarization, that is, $P \sim 0.1 \mu\text{C cm}^{-2}$, for a spin-spiral multiferroic. Unfortunately, CuO is only ferroelectric in a temperature range of 20 K, from 210 to 230 K. Here, by using a combination of density functional theory and Monte Carlo calculations, we establish that pressure-driven phase competition induces a giant stabilization of the multiferroic phase of CuO, which at 20–40 GPa becomes stable in a domain larger than 300 K, from 0 to $T > 300$ K. Thus, under high pressure, CuO is predicted to be a room-temperature multiferroic with large polarization.

¹Institut des Matériaux Jean Rouxel, UMR 6502 CNRS – Université de Nantes, Boîte Postale 32229, 44322 Nantes, Cedex 3, France. ²Institute of Materials Chemistry, Vienna University of Technology, Getreidemarkt 9/165-TC, A-1060 Vienna, Austria. ³Indian Institute of Science Education and Research (IISER) Mohali, Knowledge City, Sector 81, Mohali 140306, India. ⁴Institute of Theoretical Solid State Physics, IFW Dresden, 01171 Dresden, Germany. ⁵Institut für Theoretische Physik, Technische Universität Dresden, 01062 Dresden, Germany. Correspondence and requests for materials should be addressed to X.R. (email: Xavier.Rocquefelte@cnrs-imn.fr).

Since the first observation of multiferroicity^{1,2} in cupric oxide (CuO) by Kimura *et al.*³, it has been established that CuO is a type-II multiferroic, so that ferroelectricity occurs as a result of magnetic ordering^{3,4} and, therefore, the multiferroic ordering temperature equals the magnetic ordering temperature $T_N = 230$ K. Moreover, CuO is a quasi-one-dimensional (1D) magnetic system with a large magnetic coupling $J_z \sim 80$ meV (refs 5–7), which explains the high ordering temperature T_N . In addition, upon cooling, a polar incommensurate antiferromagnetic (AF) spin-spiral ordering, referred to as AF₂, appears below $T_N = 230$ K and a non-polar commensurate AF spin structure, AF₁, below the lock-in temperature $T_L = 213$ K. Finally, the Dzyaloshinskii–Moriya (DM) ‘cycloidal’ interactions have been shown to have a major role in the emergence of the electric polarization in CuO^{8–10}. Different aspects of the interplay between the magnetic, orbital and electronic degrees of freedom in CuO have been studied intensely^{8–14}. Recently, we have shown that by applying a pressure of 8.8 GPa to CuO¹⁴, the magnetic exchange interactions can increase by 46%. This holds the promise that under pressure T_N will increase, perhaps even to room temperature (RT). Indeed, the monoclinic phase of CuO is known to be stable up to at least 70 GPa¹⁵, even if detailed structural refinements are only available at pressures lower than 10 GPa¹⁶. Establishing the stability of the multiferroic phase under pressure, this topic not only requires a calculation of the magnetic exchange interactions by density functional theory (DFT) but also a determination of T_L , T_N and the temperature dependence of the polarization P by complementary methodologies.

Here we establish that pressure-driven phase competition renders CuO multiferroic at RT with a large P . For this, we employ both a semi-empirical ansatz as well as unbiased classical Monte Carlo (MC) simulations. More specifically, using a combination of DFT and MC calculations, we demonstrate that upon applying pressure the effective magnetic dimensionality

initially decreases, passes through a minimum and subsequently increases, the magneto-crystalline anisotropy (MAE) is reduced and the stability range of the multiferroic state strongly increases by lowering T_L and increasing T_N .

Results

Pressure effect on the magnetic exchange parameters. CuO consists of corner- and edge-sharing square-planar CuO₄ units, which form $(-\text{Cu}-\text{O}-)_{\infty}$ zigzag chains running along the [10–1] and [101] directions of the unit cell¹⁷. The low-T magnetic structure, AF₁, consists of Cu moments arranged antiferromagnetically along [10–1] and ferromagnetically along [101], with the [010] direction as the easy axis¹⁸. The exchange interactions are captured by the Heisenberg Hamiltonian $H_H = \sum_{ij} J_{ij} \mathbf{S}_i \cdot \mathbf{S}_j$, which, to properly describe the magnetic properties of CuO, requires at least five magnetic exchange coupling parameters, that is, four superexchange interactions (J_a , J_b , J_x and J_z) and one super-superexchange interaction (J_{2a})^{7,14,19,20} (see Fig. 1a). The pressure dependence of the unit cell volume and of the J -values is shown in Fig. 1b, c, respectively.

The predictive power of our DFT geometry optimization is confirmed by its capacity to reproduce the volume decrease with pressure as reported up to 17 GPa for nanocrystalline CuO samples²¹. The pressure dependence of the J -values, determined for the optimized atomic structures, compare very well with previous calculations¹⁴, that use the available experimental structures up to 8.8 GPa (ref. 16). Most importantly, J_z strongly increases, whereas J_{2a} is nearly constant for pressures up to ~ 20 GPa, after which they increase in a similar manner as J_z . Of the three smaller J -values, J_a is most affected by pressure and becomes ferromagnetic beyond about 2 GPa. The magnetic frustration, that is, the competition between J_a and J_{2a} (ref. 14), is therefore strongly enhanced by pressure. The change in ratio between the two largest J -values, that is, J_z/J_{2a} , evidences that the

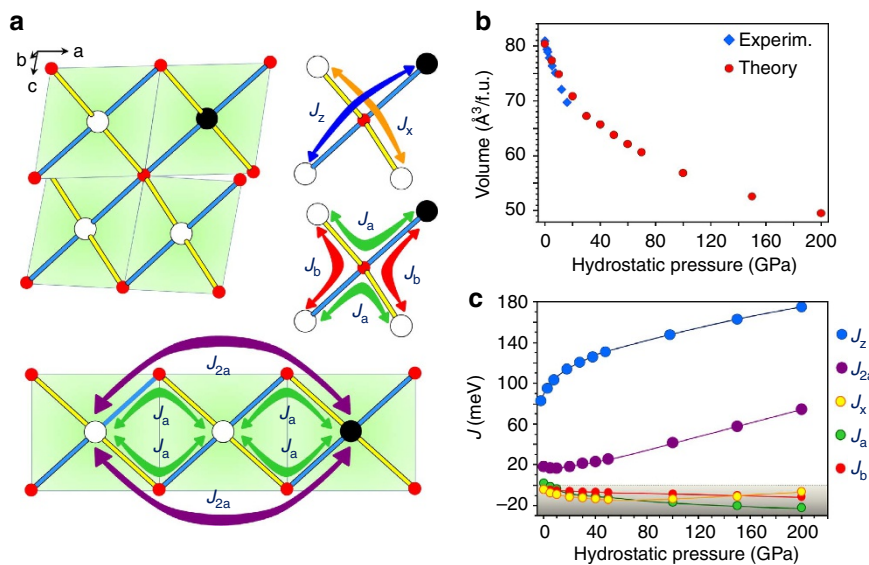


Figure 1 | High-pressure evolution of the structural and magnetic properties of CuO. (a) Schematic view of the tetrahedral environment of oxygen atoms in CuO and definition of the largest (J_z) and smaller magnetic superexchange couplings (J_x , J_a and J_b). The super-superexchange magnetic coupling, J_{2a} , corresponds to the second-neighbour interaction of the edge-sharing chains, defined by the first-neighbour interaction, J_a . Oxygen atoms are represented by small red dots, and the Cu^{2+} sites are depicted as filled and open dots, representing up-spin and down-spin, respectively. (b) Pressure dependence of the volume of CuO. The experimental values, deduced from a Birch–Murnaghan equation of state fitted to data of nanocrystalline CuO up to a pressure of 17 GPa (ref. 21), are compared with those calculated by DFT. (c) Pressure dependence of the magnetic exchange couplings of CuO. Positive and negative values represent antiferromagnetic and ferromagnetic interactions, respectively. The J 's in the grey area are ferromagnetic. The uncertainty in the DFT J_{ij} values is between 1.2 and 2.5 meV (that is, smaller than the symbols).

effective magnetic dimensionality is also affected by pressure. As shown in Fig. 2a, the quasi-1D character of the magnetic structure is enhanced for pressures up to 20 GPa but then is reduced.

Pressure effect on the Néel temperature. Having determined the pressure dependence of the magnetic exchange coupling constants, we calculate the multiferroic ordering temperature T_N up to 200 GPa. We first evaluate it using the semi-empirical random phase approximation (RPA) expression for the quasi-1D AF Heisenberg model on a cubic lattice with intrachain and interchain couplings J and J' , respectively²². The resulting T_N is shown in Fig. 2b. Choosing the parameterization such that it reproduces the transition temperature $T_N = 230$ K at ambient pressure, we observe a monotonic and substantial increase of T_N with pressure. This result coincides with the experimental pressure dependence of T_N , as was measured up to 1.8 GPa (ref. 23) and reaches RT at ~ 20 GPa.

Pressure effect on the magnetic anisotropy. To substantiate this prediction, however, one needs to go beyond the semi-empirical approach. For this purpose, we employed a classical MC technique to explore the competition between the different magnetic states as a function of both pressure and temperature, with the Hamiltonian $H = H_H + H_{UA} + H_{DM} + H_{MA}$, where H_H is the Heisenberg exchange, H_{UA} is uniaxial anisotropy (UA), H_{DM} the Dzyaloshinskii Moriya (DM) term and H_{MA} is the multiaxial (MA) anisotropy term. All these terms are relevant, but in

particular the anisotropy terms are shown by our DFT calculations to be crucial for describing the effects of pressure. The relevant magneto-crystalline anisotropy energies (MAEs) of CuO have been calculated for the ground-state (GS) AF₁ magnetic structure with $MAE = E[uvw] - E[010]$, where $E[uvw]$ is the energy deduced from spin-orbit (SO) calculations with the magnetization along the $[uvw]$ crystallographic direction. Figure 3a shows the anisotropy energy surface²⁴ for CuO in the AF₁ magnetic order at a pressure of 0 GPa. Two minima are observed along the $[010]$ direction and equivalently $[0\bar{1}0]$ direction. Thus, the SO DFT calculations properly predict that the b axis is the easy axis of magnetization of CuO for the low-T magnetic phase AF₁. A similar result is obtained for the entire pressure domain, that is, from 0 to 200 GPa. However, the MAE values are rapidly decreasing with pressure as evidenced in Fig. 3b, in which the MAE in the (a,c) plane is plotted as a function of the angle φ , such that $\varphi = 0^\circ$ corresponds to the $[101]$ direction. It also turns out that the hardest axis of magnetization (largest MAE value) is close to the $[10\bar{1}]$ direction, that is, the antiferromagnetic direction. The pressure dependence of the MAE approximately follows an exponential decay, as is illustrated in Fig. 3c for the $[-101]$ direction.

Pressure effect on the electronic polarization. Before discussing the MC data, we can estimate the order of magnitude of the ferroelectric polarization, P , by using the empirical formula proposed by Katsura *et al.*²⁵: $P = (V/\Delta)^3$, where V is the Cu–O electronic overlap integral and Δ is the p–d splitting. The

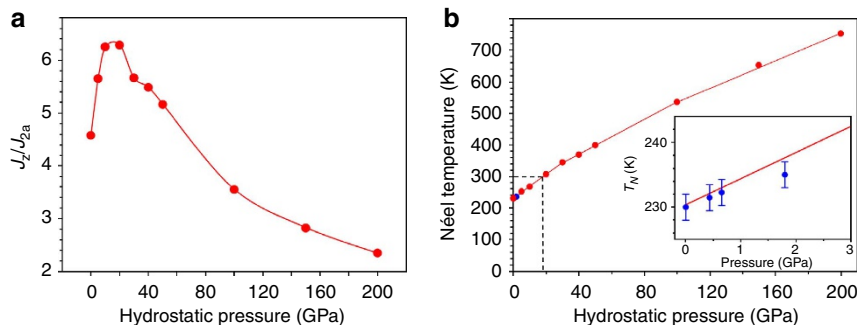


Figure 2 | High-pressure evolution of the effective magnetic dimensionality and Néel temperature of CuO. (a) Ratio between the two largest magnetic exchange interactions (J_z/J_{2a}). The 1D character of the magnetic structure is first enhanced with pressure (up to 20 GPa) and is then reduced. (b) Pressure dependence of the Néel temperature of CuO. Experimental data (in blue) measured up to 1.8 GPa (ref. 23) are compared with the result of the semi-empirical RPA expression (in red) for quasi-1D antiferromagnets²². The inset provides a zoomed view for pressure values smaller than 3 GPa. The experimental error bar²³ of about ± 2 K, estimated from a high-pressure neutron diffraction investigation, is shown using blue bars.

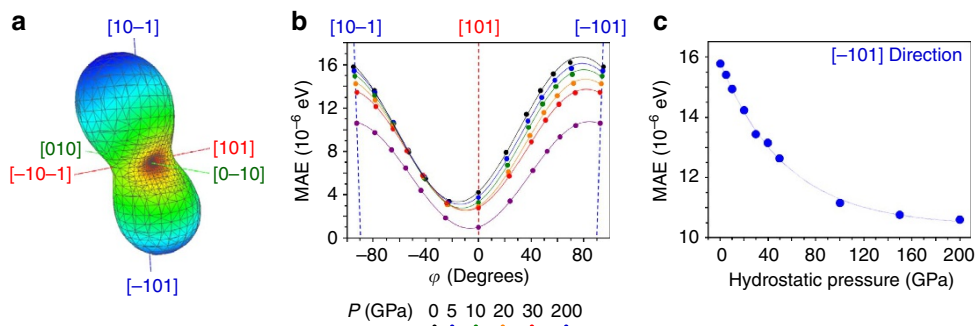


Figure 3 | High-pressure evolution of the magneto-crystalline anisotropy of CuO. MAE of CuO calculated for the GS AF₁ magnetic structure⁷ where $MAE = E[uvw] - E[010]$ and $E[uvw]$ is the energy deduced from SO calculations with magnetization along the $[uvw]$ crystallographic direction. (a) The three-dimensional shape of MAE shows that the easy axis of magnetization at 0 GPa is the b axis, that is, $[010]$ direction of the crystallographic cell. (b) MAE in the plane normal to the b axis, which is reduced by pressure. (c) Exponential decay of MAE with pressure, as illustrated for the $[-101]$ direction.

superexchange parameter is approximately given by, $J = V^4/\Delta^3$. The relevant superexchange interactions for the ferroelectric nature of CuO are J_a and J_b . Therefore, taking $J = 5$ meV and $\Delta = 1.4$ eV (refs 7,26), we find $P = 0.15 \mu\text{C cm}^{-2}$, which is close to the experimental value²⁷ of about $0.1 \mu\text{C cm}^{-2}$. Alternatively, we can estimate the ferroelectric polarization directly from our DFT calculations using the Berry phase method²⁸. As previously demonstrated theoretically⁸, the lattice contribution to the polarization (P_l) is small compared with the electronic one (P_e) in CuO, that is, $P_l \sim 0.050 \mu\text{C cm}^{-2}$ and $P_e \sim 0.200 \mu\text{C cm}^{-2}$. Here, taking into account the SO coupling, P_e was calculated to be $0.286 \mu\text{C cm}^{-2}$ at 0 GPa. It should be noted that we find an electronic polarization along the b direction ($P_e \sim 0$ along a and c directions), in good agreement with the experiments.

To determine the pressure effect on the value of P_e , we have considered two other pressure values, that is, 20 and 40 GPa. Our calculations show that $P_e = 0.286, 0.379$ and $0.455 \mu\text{C cm}^{-2}$ at 0, 20 and 40 GPa, respectively, and at zero temperature. These polarization values are along the b direction, and under pressure the polarization along the a and c directions remains zero. This clearly confirms that applying pressure on CuO leads to an increase of the electric polarization, which is predicted to be along the b direction only.

Discussion

The finite temperature MC simulations use the J -values obtained from the DFT calculations and, in particular, incorporate the H_{MA} term that is rapidly decreasing with pressure. Figure 4a shows the resulting spin current as a function of pressure, which is a quantity that is directly proportional to P . We observe that at ambient pressure close to the paramagnetic to AF1 transition, a spontaneous polarization is induced. This polarization is found to be non-zero between $T_N = 200$ and $T_L = 150$ K, which compares well with the experimentally observed stability domain of the incommensurate AF₂ magnetic order, between $T_N = 230$ and $T_L = 213$ K.

The fact that the calculated values are somewhat lower than the experimental ones is due to the model approximations involved and indicates that the MC results are conservative in the sense that they rather tend to underestimate the stability of the multiferroic phase. When the pressure is increased the polarization grows, in agreement with our DFT result for P_e dependence with pressure, and extends to a larger temperature range. For instance, at 30 GPa an increase of about 20% is observed with

respect to the polarization at 0 GPa, and the temperature range is larger and in between 245 and 115 K. At 200 GPa, the multiferroic phase (AF₂) extends down to zero temperature and the ferroelectric polarization is more than doubled. The MC results confirm the increase of T_N with pressure, in accordance with the experimental observations for pressures up to 2 GPa and the results from the semi-empirical RPA expressions. We find good quantitative agreement for the values of the differential pressure increase of T_N from experiment, 2.7 (0.2) K GPa^{-1} (ref. 23), and from the RPA and MC results, 3.5 (0.3) K GPa^{-1} and 3.0 (0.3) K GPa^{-1} , respectively. The calculated temperature–pressure phase diagram of CuO (see Fig. 4b) shows, in addition, a monotonic decrease of T_L with pressure. As a consequence, the non-polar AF₁ phase disappears from the phase diagram with increasing pressure, at the benefit of the multiferroic AF₂ phase. The MC simulations indicate that T_N reaches RT at ~ 40 GPa, which is higher than the ~ 20 GPa, obtained from the semi-empirical RPA expressions, underlining that the MC pressure of ~ 40 GPa is a conservative estimate for the critical pressure value.

Finally, the present temperature–pressure phase diagram of CuO evidences under high pressure a large increase of the stability range of the incommensurate multiferroic AF₂ phase, which is stable in a domain of only 20 K (from 210 to 230 K) at 0 GPa, and in a domain larger than 300 K (from 0 to $T > 300$ K) at 20–40 GPa. Such a giant stabilization of a multiferroic phase by pressure has never been observed or proposed. Indeed, except for CuO, all the reported pressure–temperature phase diagrams of multiferroic materials ($\text{Ni}_3\text{V}_2\text{O}_8$, MnWO_4 , TbMnO_3 and RMn_2O_5 with $R = \text{Tb, Dy, Ho} \dots$)^{29–32} lead to the same conclusion, namely that the stability range of the incommensurate magnetic phase is reduced by pressure. The fact that our theoretical and predictive approach correctly reproduces the experimental low-pressure results gives considerable credit to our predictions. In contrast to the multiferroic compounds mentioned above, the geometrical modifications (bond distances and angles) under pressure in CuO induce an increase of the magnetic frustration, as previously demonstrated up to 8.8 GPa (ref. 14) and confirmed here for a larger pressure domain from 0 to 200 GPa. Further theoretical efforts on the dependence of the magnetic frustration versus pressure (chemical or physical) in CuO and the related compounds is clearly needed and will be of direct interest in the quest of type-II multiferroics with tunable ferroelectric and magnetic properties.

The first RT binary multiferroic material is thus within reach: CuO at pressures of 20–40 GPa. To be practical, for technical

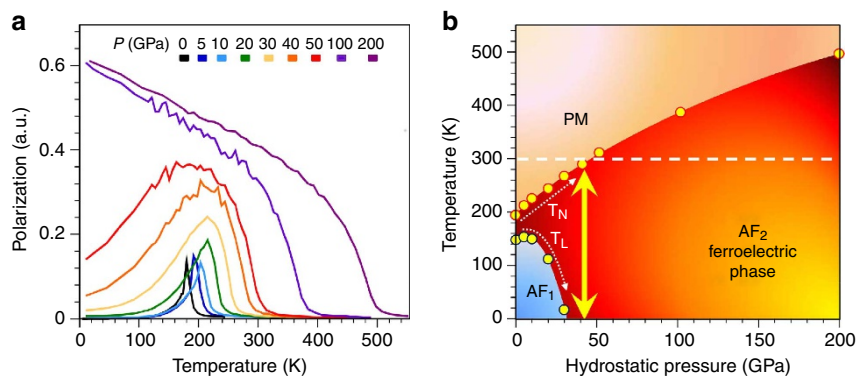


Figure 4 | Temperature–pressure phase diagram of the magnetic model of CuO. Magnetic and ferroelectric properties of CuO as determined by MC calculations, based on the microscopic magnetic interactions. **(a)** Temperature dependence of the ferroelectric polarization, which is proportional to the calculated spin current, for different values of hydrostatic pressure. **(b)** Temperature–pressure magnetic phase diagram of CuO. The RT is indicated by the horizontal white dashed line and the giant stabilization of the AF₂ ferroelectric phase of CuO is highlighted by the vertical yellow double arrow. PM stands for paramagnetic.

applications, the high-pressure form of CuO must be made stable at ambient conditions. To achieve this, there are at least two strategies. Very special for CuO is the possibility to stabilize its high pressure form at a nanoscale level by applying high-energy ion irradiation at high pressures³³. In such experiments, the quenched high-pressure structure remains even after releasing pressure. Another promising strategy can be a core-shell synthesis³⁴ according to which CuO nanoparticles are embedded in a shell material that has a negative thermal expansion coefficient, which then acts as an effective pressure medium for the CuO core.

Methods

DFT calculations. The DFT calculations have been carried out by using two different codes: Vienna Ab initio Simulation Package (VASP)³⁵ for the geometry optimization at the different pressure values and WIEN2k programme package³⁶ for the calculation of the magnetic exchange, J_{ij} , and magneto-crystalline anisotropy energy, MAE, values.

For the geometry optimizations, a 16 formula units cell has been used, that is, $2a \times 2b \times 2c$, with a , b and c being the crystallographic cell parameters. The GS magnetic order (AF₁) has been considered for the geometry optimization. The parameters used in the VASP calculations are the following. We have used the GGA + U approach with $U_{\text{eff}} = 6.5$ eV for the Cu(3d) states, as in our previous investigation^{8,20}. It allows having a proper description of the structural properties of CuO. The wave functions are expanded in a plane wave basis set with kinetic energy below 500 eV. The VASP package is used with the projector augmented wave method of Blöchl³⁷. The integration in the Brillouin Zone is done by the Methfessel–Paxton method³⁸ on a $3 \times 3 \times 3$ set of k -points determined by the Monkhorst–Pack scheme³⁹. All atoms were then allowed to relax by following a conjugate gradient minimization of the total energy scheme (3×10^{-2} eV Å⁻¹).

The magnetic exchange parameters (J_{ij} values) were estimated based on the optimized atomic structures and for each pressure (from 0 to 200 GPa), and using the WIEN2k programme package with the onsite PBE0 (ref. 40) hybrid functional for 8 and 32 *f.u.* cells. The J_{ij} values have been deduced from a least-squares fit procedure and the quality of the fits is shown in Fig. 5a,b. It should be noticed that the choice of the PBE0 onsite hybrid functional in WIEN2k was motivated by its ability to properly reproduce the magnetic exchange coupling in a series of copper oxide compounds and its dependence with the Cu–O–Cu bond angle¹⁴.

The MAE value has been estimated for the AF₁ GS magnetic structure, using the code WIEN2k with the PBE0 hybrid functional and including the SO coupling. MAE corresponds to an energy difference between two directions of the magnetization density. Here we use the [010] direction, that is, the easy axis, as the reference:

$$\text{MAE} = E[\text{uvw}] - E[010] \quad (1)$$

$E[\text{uvw}]$ is the energy deduced from SO calculations with magnetization along the [uvw] crystallographic direction. It should be noticed that MAE is very sensitive to the k -mesh. The quality of the k -mesh has been carefully chosen, leading to the use of a $5 \times 12 \times 6$ set of k -points for the 8 *f.u.* cell.

The electronic contribution (P_e) to the polarization P was evaluated using the Berry phase approach²⁸. As previously shown⁸, the lattice contribution (P_l) is small compared with the electronic one (P_e) in CuO: $P_e \sim 0.200 \mu\text{C cm}^{-2}$ and $P_l \sim 0.050 \mu\text{C cm}^{-2}$. Here we have redone such calculations using the VASP code with the GGA + U formalism and a U_{eff} value of 7.5 eV, to match the J_{ij} values obtained using the PBE0 hybrid functional in our WIEN2k calculations. The non-collinear magnetic structure, AF₂, previously discussed in ref. 8 has been used. To have adequate electric polarization values, it was crucial to turn on the SO coupling

during the structural relaxation. Indeed, at 0 GPa, $P_e = 0.053$ and $0.286 \mu\text{C cm}^{-2}$, respectively, for the atomic structure relaxed without and with SO.

Estimation of T_N based on the RPA formula

$$J' = T_N / \left[4c \sqrt{\ln\left(\frac{\alpha J}{T_N}\right) + \frac{1}{2} \ln \ln\left(\frac{\alpha J}{T_N}\right)} \right] \quad (2)$$

The above equation has been developed for the estimation of T_N of a quasi-1D AF Heisenberg model on a cubic lattice with J and J' , the intrachain and interchain couplings, respectively²². The related GS magnetic order leads to the following energy expression:

$$E(\text{GS}) = J + 2J' \quad (3)$$

Although CuO is a quasi-1D magnetic system, it exhibits a more complex magnetic order due to the low symmetry of its atomic structure (monoclinic space group: C2/c). As a consequence, its GS magnetic order (AF₁) leads to the following energy expression:

$$E(\text{AF}_1) = J_z - J_x + J_2 \text{ with } J_2 = J_{2a} + J_{2b} + J_{2c} \quad (4)$$

with J_{2a} being the predominant super-superexchange interaction. For more details, see (refs 7 and 20). Considering $E(\text{GS}) = E(\text{AF}_1)$ and J_z as the intrachain coupling, that is, $J_z = J$, we can define J' as:

$$2J' = -J_x + J_2 \quad (5)$$

Our detailed results are illustrated in Fig. 6.

Classical MC simulations. The model Hamiltonian used in MC simulations is given by,

$$H = H_H + H_{UA} + H_{DM} + H_{MA}, \quad (6)$$

where, H_H is the Heisenberg part, H_{UA} is UA term, H_{DM} is DM term and H_{MA} is the MA anisotropy. The Heisenberg term and the UA term can be written together as,

$$H_H + H_{UA} = \sum_{ij} J_{ij}^p \mathbf{S}_i \cdot \mathbf{S}_j \quad (7)$$

where J_{ij}^p refer to exchange parameters at pressure P . The various exchange parameters are J_x, J_y, J_{2a}, J_4 and J_b (see Fig. 1a). The UA term has been included in the Heisenberg part by making the following replacement:

$$J_z \mathbf{S}_i \cdot \mathbf{S}_j \rightarrow J_z \left[S_i^x S_j^x + (1 + \lambda) S_i^y S_j^y + S_i^z S_j^z \right] \quad (8)$$

This allows a lower energy for a collinear AF₁ state in which all the spins are aligned along the y axis. The DM term is given by

$$H_{DM} = D \sum_{ij} \hat{x} \cdot (\mathbf{S}_i \times \mathbf{S}_j) \quad (9)$$

As we are mainly interested in the competition between two magnetic states, the collinear AF₁ and the non-collinear AF₂, we restrict the spins to reside in y - z plane only. Therefore, we only introduce a DM vector pointing along x direction. The experimental observation that the AF₂ state is stable in a narrow temperature window between 230 and 213 K is reproduced in an effective manner by introducing a MA anisotropy term, in the Hamiltonian of the form²⁴,

$$H_{MA} = B \sum_i (S_i^y S_i^z)^2 \quad (10)$$

The Heisenberg term, H_H , alone leads to a degeneracy of GSs. The GS manifold consists of perfectly ordered, interpenetrating sub-lattices with vector order parameters whose relative orientation is left completely undetermined by the

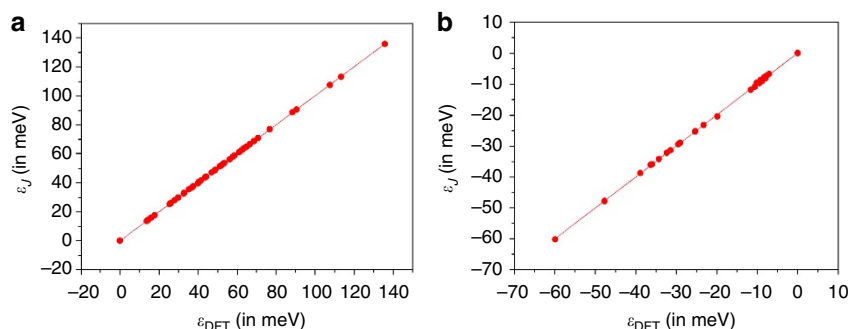


Figure 5 | Quality of the DFT magnetic exchange parameters. Graphical representation of the quality of the least-squares fit procedure for the 8 (a) and 32 (b) formulae units models. ε_{DFT} and ε_j are, respectively, the relative energies (with respect to AF₁) deduced from the DFT calculations and the J parameters. The s.d. values are 0.12 and 0.25 meV, respectively, for the 8 and 32 *f.u.* models.

Heisenberg term alone. The UA term prefers a collinear magnetic state, where the two sub-lattice order parameters align along the y axis. This is precisely the experimentally observed AF₁ state of CuO. The DM coupling favours a non-collinear (but coplanar) state and, therefore, it competes with the H_{UA} . There is a critical strength of the DM coupling, D_c , above which the AF₁ is not the GS. Given that the AF₁ is the GS at ambient pressure, we conclude that $D < D_c$.

We use the Metropolis algorithm to perform Markov Chain MC simulations on classical spins. The simulations are started with a completely random spin configuration at high temperature. Because of the presence of many competing interactions and nearly degenerate GSs, the simulations require a large number of equilibration and averaging steps. We use $\sim 10^6$ MC steps for equilibration and a similar number of steps for averaging at each temperature. The temperature is then reduced in small steps (~ 5 K) and the system is allowed to anneal towards the GS spin configuration. The main quantity of interest is the spin current, which is defined as $\langle \mathbf{e}_{ij} \times (\mathbf{S}_i \times \mathbf{S}_j) \rangle$, where \mathbf{e}_{ij} is a vector connecting spins \mathbf{S}_i and \mathbf{S}_j , and the angular brackets denote thermal as well as spatial average. The ferroelectric polarization is proportional to the spin current with a prefactor estimated to be $0.150 \mu\text{C cm}^{-2}$ following Katsura *et al.*²⁵

The simulations are carried out on lattices with $N = 12^3$ sites. We have checked the stability of our results for larger sizes (up to $N = 32^3$) for selected values of pressure (Supplementary Fig. S1). The procedure used to estimate T_L and T_N for 2 pressures (0 and 30 GPa) is shown in Fig. 7.

The UA parameter $\lambda = 0.02$ is kept constant. The MA anisotropy B decreases exponentially with increasing pressure; we use $B = 500 e^{-P/10}$ ($B = 500$ for $P = 0$

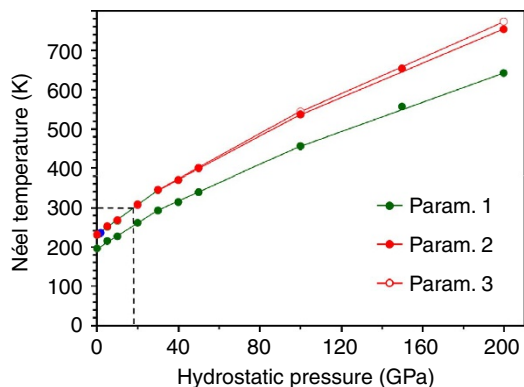


Figure 6 | High-pressure evolution of the Néel temperature of CuO.

Pressure dependence of the Néel temperature of CuO. Experimental data measured up to 1.8 GPa are compared with theoretical ones deduced from an analytical expression developed for $S = 1/2$ quasi-1D Heisenberg antiferromagnets²². Three parameterizations are used, the original one with $c = 0.233$ and $\alpha = 2.6$ (param.1) and two modified forms, with $c = 0.284$ and $\alpha = 2.6$ (param.2) and with $c = 0.233$ and $\alpha = 8.4$ (param.3). The black dash line evidences that T_N is reaching RT at about 20 GPa (from both param. 2 and 3).

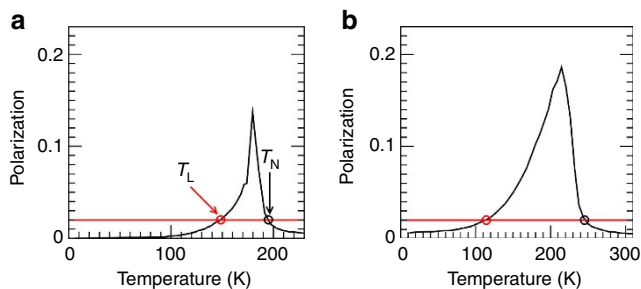


Figure 7 | Temperature dependence of the spin current. The spin current is proportional to ferroelectric polarization and is given for two sets of parameters corresponding to $P = 0$ GPa (a) and $P = 30$ GPa (b). An increase in spin current upon decreasing temperature is an indication of the onset of a non-collinear ferroelectric phase. The decrease of spin current below a cutoff value is defined at the transition to a collinear state. We show the red horizontal line ($P = 0.02$) as the cutoff value used for inferring T_N and T_L .

and $B = 24.9$ for $P = 30$). The exponential decrease is motivated by the DFT results presented in Fig. 3. The large value of B at $P = 0$ is required to obtain the narrow range of stability of AF₂ state at high temperatures. Although UA term is also decreasing with pressure, this does not lead to any crucial changes in the phase diagram shown in Fig. 4. We also keep the DM coupling fixed to $D = 0.8D_c$. The choice of the parameter D is not very crucial, as long as D is smaller than D_c . To illustrate this point, we show the results for spin current for various values of D at $P = 0$ GPa and $P = 30$ GPa in Supplementary Fig. S2.

References

- Cheong, S. W. & Mostovoy, M. Multiferroics: a magnetic twist for ferroelectricity. *Nat. Mater.* **6**, 13–20 (2007).
- Scott, J. F. Applications of magnetoelectrics. *J. Mater. Chem.* **22**, 4567–4574 (2012).
- Kimura, T., Sekio, Y., Nakamura, H., Siegrist, T. & Ramirez, A. P. Cupric oxide as an induced-multiferroic with high-TC. *Nat. Mater.* **7**, 291–294 (2008).
- Mostovoy, M. Transition metal oxides: multiferroics go high- T_c . *Nat. Mater.* **7**, 269–270 (2008).
- Ain, M., Reichardt, W., Hennion, B., Pepy, G. & Wanklyn, B. M. Magnetic excitations in CuO. *Phys. C* **162–164**, 1279–1280 (1989).
- Boothroyd, A. T. High-Energy magnetic excitations in CuO. *Phys. B* **234–236**, 731–733 (1997).
- Rocquefelte, X. *et al.* Short-range magnetic order and temperature-dependent properties of cupric oxide. *J. Phys. Condens. Matter* **21**, 045502 (2010).
- Giovannetti, G. *et al.* High-TC ferroelectricity emerging from magnetic degeneracy in cupric oxide. *Phys. Rev. Lett.* **106**, 026401 (2011).
- Tolédano, P. *et al.* Theory of high-temperature multiferroicity in cupric oxide. *Phys. Rev. Lett.* **106**, 257601 (2011).
- Jin, G. *et al.* Origin of ferroelectricity in high- T_c magnetic ferroelectric CuO. *Phys. Rev. Lett.* **108**, 187205 (2012).
- Scagnoli, V. *et al.* Observation of orbital currents in CuO. *Science* **332**, 696–698 (2011).
- Johnson, S. L. *et al.* Femtosecond dynamics of the collinear-to-spiral antiferromagnetic phase transition in CuO. *Phys. Rev. Lett.* **108**, 037203 (2012).
- Villarreal, R. *et al.* Magnetic phase diagram of CuO via high-resolution ultrasonic velocity measurements. *Phys. Rev. Lett.* **109**, 167206 (2012).
- Rocquefelte, X., Schwarz, K. & Blaha, P. Theoretical investigation of the magnetic exchange interactions in copper(II) oxides under chemical and physical pressures. *Sci. Rep.* **2**, 759 (2012).
- Bourne, L. C., Yu, P. Y., Zettl, A. & Cohen, M. L. High-pressure electrical conductivity measurements in the copper oxides. *Phys. Rev. B* **40**, 10973 (1989).
- Ehrenberg, H., McAllister, J. A., Marshall, W. G. & Attfield, J. P. Compressibility of copper-oxygen bonds: a high-pressure neutron powder diffraction study of CuO. *J. Phys. Condens. Matter* **11**, 6501–6508 (1999).
- Åsbrink, S. & Norrby, L.-J. A refinement of crystal structure of copper(II) oxide with a discussion of some exceptional e.s.d.'s. *Acta. Crystallogr. B* **26**, 8–15 (1970).
- Forsyth, J. B., Brown, P. J. & Wanklyn, B. M. Magnetism in cupric oxide. *J. Phys. C* **21**, 2917–2929 (1989).
- Filippetti, A. & Fiorentini, V. Magnetic ordering in CuO from first principles: a cuprate antiferromagnet with fully three-dimensional exchange interactions. *Phys. Rev. Lett.* **95**, 086405 (2005).
- Rocquefelte, X., Schwarz, K. & Blaha, P. Comment on “High-TC ferroelectricity emerging from magnetic degeneracy in cupric oxide”. *Phys. Rev. Lett.* **107**, 239701 (2011).
- Wang, Z. *et al.* X-ray diffraction and Raman spectroscopic study of nanocrystalline CuO under pressures. *Solid State Commun.* **121**, 275–279 (2002).
- Yasuda, C. *et al.* Néel temperature of quasi-low-dimensional Heisenberg antiferromagnets. *Phys. Rev. Lett.* **94**, 217201 (2005).
- Chatterji, T., Brown, P. J. & Forsyth, J. B. High pressure neutron diffraction investigation of CuO. *J. Phys. Condens. Matter* **17**, S3057–S3062 (2005).
- Herak, M. Cubic magnetic anisotropy of the antiferromagnetically ordered Cu_3TeO_6 . *Solid State Commun.* **151**, 1588–1592 (2011).
- Katsura, H., Nagaosa, N. & Balatsky, A. V. Spin current and magnetoelectric effect in noncollinear magnets. *Phys. Rev. Lett.* **95**, 057205 (2005).
- Ghijsen, J. *et al.* Electronic structure of Cu_2O and CuO. *Phys. Rev. B* **38**, 11322–11330 (1988).
- Babkevich, P. *et al.* Electric field control of chiral magnetic domains in the high-temperature multiferroic. *Phys. Rev. B* **85**, 134428 (2012).
- Malashevich, A. & Vanderbilt, D. First principles study of improper ferroelectricity in TbMnO_3 . *Phys. Rev. Lett.* **101**, 037210 (2008).
- Chaudhury, R. P. *et al.* Pressure-temperature phase diagram of multiferroic $\text{Ni}_3\text{V}_2\text{O}_8$. *Phys. Rev. B* **75**, 012407 (2007).
- Chaudhury, R. P. *et al.* Thermal expansion and pressure effect in MnWO_4 . *Phys. B* **403**, 1428–1430 (2008).

31. Makarova, O. L. *et al.* Pressure-induced change in the magnetic ordering of TbMnO₃. *Phys. Rev. B* **84**, 020408 (2011).
32. Noda, Y. *et al.* Magnetic and ferroelectric properties of multiferroic RMn₂O₅. *J. Phys. Condens. Matter* **20**, 434206 (2008).
33. Lang, M. *et al.* Nanoscale manipulation of the properties of solids at high pressure with relativistic heavy ions. *Nat. Mater.* **8**, 793–797 (2009).
34. Zhao, W. *et al.* Fabrication of uniform magnetic nanocomposite spheres with a magnetic core/mesoporous silica shell structure. *J. Am. Chem. Soc.* **127**, 8916–8917 (2005).
35. Kresse, G. & Furthmüller, J. Efficient iterative schemes for ab initio total-energy calculations using a plane-wave basis set. *Phys. Rev. B* **54**, 11169 (1996).
36. Blaha, P., Schwarz, K., Madsen, G., Kvasnicka, D. & Luitz, J. *WIEN2k: An Augmented Plane Wave + LO Program for Calculating Crystal Properties* (TU Wien, Vienna, 2001).
37. Blöchl, P. E. Projector augmented-wave method. *Phys. Rev. B* **50**, 17953 (1994).
38. Methfessel, M. & Paxton, A. T. High-precision sampling for Brillouin-zone integration in metals. *Phys. Rev. B* **40**, 3615 (1989).
39. Monkhorst, H. J. & Pack, D. Special points for Brillouin-zone integrations. *Phys. Rev. B* **13**, 5188 (1976).
40. Perdew, J. P., Ernzerhof, M. & Burke, K. Rationale for mixing exact exchange with density functional approximations. *J. Chem. Phys.* **105**, 9982–9985 (1996).

Acknowledgements

X.R. thanks the IMN (Nantes) and the CCIPL (Centre de Calcul Intensif des Pays de la Loire) for computing facilities. S.K. acknowledges the use of High Performance Computing Facility at IISER Mohali, and support from DST, India. P.B. was supported by the Austrian Science Foundation FWF (SFB F41 'Vicom').

Author contributions

X.R. designed and performed the DFT calculations. X.R. wrote the paper with contributions from all co-authors. S.K. performed the MC simulations. All co-authors contributed to analysing and discussing the results.

Additional information

Supplementary Information accompanies this paper at <http://www.nature.com/naturecommunications>

Competing financial interests: The authors declare no competing financial interests.

Reprints and permission information is available online at <http://npg.nature.com/reprintsandpermissions/>

How to cite this article: Rocquefelte, X. *et al.* Room-temperature spin-spiral multiferroicity in high-pressure cupric oxide. *Nat. Commun.* **4**:2511 doi: 10.1038/ncomms3511 (2013).